

## HYBRID ATMOSPHERES AND WINDS IN SUPERGIANT STARS

L. HARTMANN, A. K. DUPREE, AND J. C. RAYMOND

Harvard-Smithsonian Center for Astrophysics

Received 1979 November 8; accepted 1979 December 19

### ABSTRACT

Ultraviolet spectra showing evidence for hybrid chromospheres and winds are found in the supergiants  $\alpha$  Aqr (G2 Ib) and  $\beta$  Aqr (G0 Ib). Characteristics of both solar-type transition regions and the cool chromospheric regions typical of later supergiants such as  $\lambda$  Vel (K5 Ib) are present. This suggests a gradual transition between activity and winds analogous to solar conditions and the cool, massive winds of luminous late-type stars.

*Subject headings:* stars: coronae — stars: late-type — stars: supergiants — stars: winds — ultraviolet: spectra

### I. INTRODUCTION

The observational evidence for mass loss in late-type luminous stars indicates a cool, low-velocity flow (Deutsch 1956, 1960; Weymann 1962). Late-type giants appear to have low chromospheric temperatures, and transition-region lines are weak or absent (Wing 1978; Linsky and Haisch 1979). On the other hand, the Sun possesses a hot, high-velocity, low-mass flux wind, and by analogy this is expected to be typical of dwarfs. The two extremes of mass loss suggest a direct correlation between temperatures and wind structure. Linsky and Haisch (1979) identified a boundary line in the H-R diagram, determining the onset of large mass loss (Reimers 1977; called the “supersonic transition locus” by Mullan 1978) with a “sharp” division between stars with transition-region ions and those without high-temperature material. They speculated that massive winds may suppress the formation of transition-region and coronal structures.

In this *Letter* we discuss the relationship between chromospheric temperatures and mass loss through *IUE* observations of three supergiants,  $\alpha$  Aqr (G2 Ib),  $\beta$  Aqr (G0 Ib), and  $\lambda$  Vel (K5 Ib). While  $\lambda$  Vel shows the expected cool chromosphere and massive wind, the G supergiants possess a hybrid structure, having both lines representative of Linsky and Haisch cool chromosphere (“nonsolar”) stars, and the transition-region lines N v, C iv, and Si iv. The Mg II lines show strong blueshifted absorption components, indicating that the presence of high-temperature material does not rule out substantial mass loss. These results, coupled with other observations showing that the transition between hot-transition-region stars and cool-chromosphere stars in the H-R diagram is not sharp (Dupree *et al.* 1979; Brown, Jordan, and Wilson 1979), and that the division between stars with evidence of mass loss in Ca II and those without is similarly blurred (Stencel 1978), indicate a more gradual transition between solar-type winds and cool winds.

### II. OBSERVATIONS

Short-wavelength (1200–1950 Å) and long-wavelength (2000–3200 Å) spectra of  $\alpha$  Aqr,  $\beta$  Aqr, and  $\lambda$  Vel were taken with the *IUE* satellite, in the low-dispersion format ( $\sim 6$  Å resolution) for all short-wavelength exposures, and high dispersion ( $\sim 0.2$  Å resolution) at long wavelengths. All exposures were in the large aperture. Details of the instrumentation and performance can be found in Boggess *et al.* (1978). The spectra have been approximately corrected for the flux error originally present in the original *IUE* reductions (Holm 1979).

#### a) $\lambda$ Velorum (K5 Ib)

The spectrum of  $\lambda$  Vel is shown in Figure 1; calculated line fluxes are listed in Table 1. The stellar surface fluxes were found through use of the Barnes-Evans (1973) relation, using  $V - R$  colors from the catalog of Johnson *et al.* (1966). High-temperature ions like N v and Si iv are absent by factors of 3 or more below the quiet-Sun surface flux; C iv is weak, if present. There is a feature near the wavelength of He II  $\lambda 1640$  that is more likely due to Fe II, as discussed below.

The identifications listed need to be treated with caution, because the 6 Å resolution cannot permit accurate wavelength determinations. The O I  $\lambda 1304$  multiplet, produced by resonance fluorescence with L $\beta$ , is certain, and the presence of Si II  $\lambda \lambda 1808, 1817$  seems likely. Carpenter and Wing (1979) have observed S I lines at  $\lambda \lambda 1807.3, 1820.3$  in a high dispersion spectrum of  $\alpha$  Ori (M2 Iab), in strengths greater than the Si II lines. The S I distribution in wavelength is resolvable, and Figure 1 clearly shows the  $\lambda 1826$  line as a shoulder in the  $\lambda 1810$  complex. With this identification, other S I lines arising from the ground state have been assigned to observed features, with the  $\lambda \lambda 1475, 1488,$  and  $\lambda \lambda 1900, 1914$  identifications the most attractive. Fe II identifications are suggested by observed emission lines in the long-wavelength spectra, most prominently  $\lambda \lambda 2693.63, 2756.55$  (multiplet 62). Fluorescence with

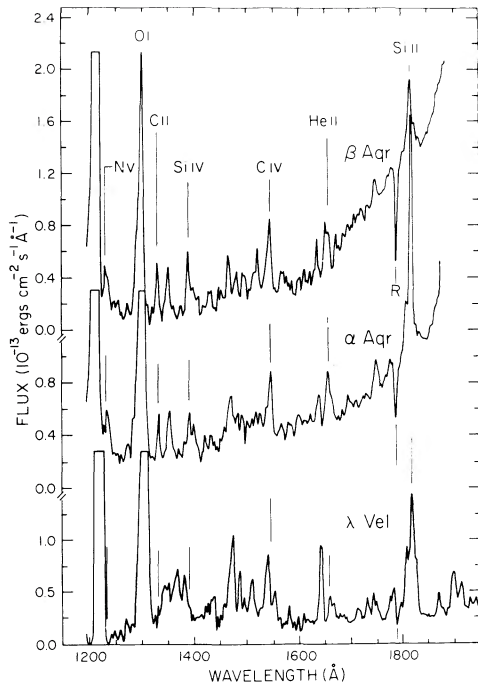


FIG. 1.—Short-wavelength IUE spectra of three late supergiants;  $\beta$  Aqr (G0 Ib),  $\alpha$  Aqr (G2 Ib), and  $\lambda$  Vel (K5 Ib). High-temperature lines of N v and C iv are present in the G supergiants, but not in  $\lambda$  Vel. The G supergiants also show “cool” lines, such as  $\lambda$ 1475, that are characteristic of  $\lambda$  Vel and other late-supergiant stars.

$\text{L}\alpha$  may produce Fe II  $\lambda$ 1296 (Brown, Jordan, and Wilson 1979). Careful intercomparison of images, allowing for possible wavelength shifts in the large aperture, indicates that C II is not strongly present in the blended emission  $\sim\lambda\lambda$ 1337–1376.

#### b) $\alpha$ Aquarii (G2 Ib)

Figure 1 also contains the short-wavelength spectrum of  $\alpha$  Aqr, with line identifications and fluxes in Table 2. The group of “cool” lines near 1500 Å is present once again, with  $\lambda$ 1475 strongest and having a comparable surface flux in  $\lambda$  Vel. However, high-temperature lines make their appearance as well. N v, C iv, and Si iv are obviously present, and the feature at  $\lambda$ 1640 may be interpreted as He II. C II  $\lambda$ 1335 is strong, comparable to  $\lambda$ 1475, which is definitely not true in  $\lambda$  Vel. No evidence is seen for lines at  $\lambda\lambda$ 1826, 1900, and 1915. If they are present in the same ratio to  $\lambda$ 1475 as in  $\lambda$  Vel, it appears that  $\lambda$ 1826 should be marginally detectable, while the others would not. Unfortunately, the second SWP exposure was overexposed in this wavelength region, and it is difficult to draw a firm conclusion on the basis of one exposure. Because of the irregularity of the underlying continuum near 1900 Å, it is uncertain whether C III  $\lambda$ 1909 is present, and the flux listed in Table 1 must be considered an upper limit. The fluxes for the SWP 3587 and 3610 exposures, taken 1.7 days apart (JD = 2,443,856.61 and 858.31), show no evidence of variability.

#### c) $\beta$ Aquarii (G0 Ib)

Line strengths and identifications are similar to  $\alpha$  Aqr, as given in Table 2, and as displayed in Figure 1. The stellar surface fluxes of  $\alpha$  and  $\beta$  Aqr in the transition-region lines range from quiet-Sun values for low-temperature ions to a few times solar for high-temperature ions such as C iv and N v (Table 2). This same pattern of high-temperature enhancement has been seen in active chromosphere dwarfs (Hartmann *et al.* 1979).

#### d) Mg II Lines

Figure 2 shows the Mg II profiles of the three stars.  $\lambda$  Vel shows the standard, blueshifted absorption expected in supergiants with massive winds. However,  $\alpha$  Aqr and  $\beta$  Aqr clearly show a second, high-velocity component. Wavelength scales were established by shifting the IUE wavelengths to symmetrize the emission wings for  $\lambda$  Vel and  $\beta$  Aqr. The absorption component in  $\alpha$  Aqr strongly absorbs the blue emission near the  $k_1$  and  $h_1$  points, so we have assumed the similarity of emission to  $\beta$  Aqr in order to establish the zero-point shift in this case.

All of the stars have an absorption component centered near a blueshift  $\sim -20$  km s $^{-1}$  (relative to the emission). However, the G supergiants have much higher velocity material. The magnitude of the high-velocity shift makes it extremely unlikely that this is interstellar material, particularly considering the LSR radial velocities ( $\sim +6$  km s $^{-1}$  for  $\alpha$ ,  $\beta$  Aqr;  $+18$  km s $^{-1}$  for  $\lambda$  Vel; Abt and Biggs 1972).

The velocities listed in Table 3 refer to apparent shifts of the absorption components. This may not be simply

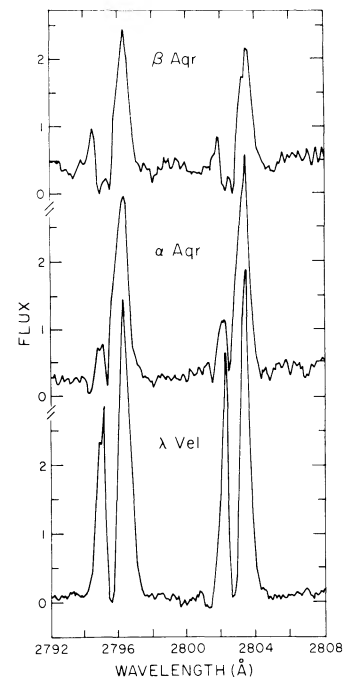


FIG. 2.—Mg II spectra of the program stars. The stars  $\alpha$  Aqr and  $\beta$  Aqr show high-velocity circumstellar absorption not present in  $\lambda$  Vel.

TABLE 1  
EMISSION LINES IN  $\lambda$  VELORUM

| $\lambda^a$        | $f_{\oplus}^b$    | $F_*^c$ | Tentative Identifications                               |
|--------------------|-------------------|---------|---|
| 1221.....          | O.E. <sup>d</sup> | ...     | L $\alpha$ 1215   |
| 1299.8b.....       | 15                | 1.6+3   | S I $\lambda$ 1295.7, 96.2 (9)+Fe II                    |
| 1307.8.....        | 48                | 5.0+3   | O I $\lambda$ 1302.2, 1304.9, 1306.0 (2)                |
| 1337.2-1355.2b.... | 6.5               | 6.7+2   | O I $\lambda$ 1356, 1359?                               |
| 1355.2-1376.4b.... | 8.2               | 8.5+2   | ....  |
| 1376.4-1395.0b.... | 7.0               | 7.2+2   | ....  |
| 1418.6-1429.2b.... | 2.9               | 3.0+2   | S I $\lambda$ 1425.1 (5)?                               |
| 1429.2-1433.2b.... | 4.4               | 4.6+2   | S I $\lambda$ 1433.3+ $\lambda$ 1436.9 (5)?             |
| 1456.2.....        | 1.7               | 1.8+2   | ....  |
| 1474.8b.....       | 11                | 1.1+3   | S I $\lambda$ 1474.8 (3)                                |
| 1488.0.....        | 4.4               | 4.6+2   | S I $\lambda$ 1488.0 (3)                                |
| 1496.0.....        | 2.9               | 3.0+2   | ....  |
| 1511.6b.....       | 6.6               | 6.8+2   | ....  |
| 1527.8.....        | 4.0               | 4.1+2   | Si II $\lambda$ 1526.7, 1533.3 (2)?                     |
| 1540.8.....        | 6.7               | 6.9+2   | ....  |
| 1554.0.....        | 4.1               | 4.2+2   | C I $\lambda$ 1560 (3)?, Fe II $\lambda$ 1558 (46)      |
| 1580.8.....        | 2.3               | 2.4+2   | Fe II $\lambda$ 1588.3, 1584.9 (44)                     |
| 1641.0.....        | 3.4               | 3.5+2   | Fe II $\lambda$ 1643.6, 1637.4 (42)                     |
| 1659.8.....        | 1.2               | 1.2+2   | C I $\lambda$ 1657 (2), Fe II $\lambda$ 1659 (41), (40) |
| 1665.6.....        | 0.8               | 8.0+1   | Fe II $\lambda$ 1670.0 (40), P I $\lambda$ 1671.7 (2)   |
| 1712.8b.....       | 0.6               | 6.0+1   | Fe II $\lambda$ 1713.0 (38)                             |
| 1731.6b.....       | 0.9               | 9+1     | ....  |
| 1744.6.....        | 0.6               | 6+1     | ....  |
| 1750.2.....        | 0.7               | 7+1     | ....  |
| 1776.4.....        | 0.6               | 6+1     | P I $\lambda$ 1779.0 (1)                                |
| 1782.0.....        | 0.9               | 9+1     | P I $\lambda$ 1782.9, 1787.7 (1)                        |
| 1808.0.....        | 2.6               | 2.7+2   | Si II $\lambda$ 1808.0+S I $\lambda$ 1807.3             |
| 1816.6.....        | 8.3               | 8.6+2   | Si II $\lambda$ 1816.9+S I $\lambda$ 1820.4             |
| 1826.8.....        | 1.2               | 1.2+2   | Si II $\lambda$ 1817.5+S I $\lambda$ 1826.3             |
| 1869.2.....        | 0.3               | 3+1     | ....  |
| 1898.6b.....       | 1.7               | 1.8+2   | S I $\lambda$ 1900.3 (1)                                |
| 1914.0b.....       | 0.9               | 9+1     | S I $\lambda$ 1914.7 (1)                                |

<sup>a</sup> b = blend.

<sup>b</sup> Flux at Earth in units of  $10^{-13}$  ergs  $\text{cm}^{-2}$   $\text{s}^{-1}$ , uncorrected for interstellar absorption.

<sup>c</sup> Flux at stellar surface in units of ergs  $\text{cm}^{-2}$   $\text{s}^{-1}$ , where the form  $a + \alpha$  implies  $a \times 10^\alpha$ .

<sup>d</sup> O.E. = overexposure.

TABLE 2  
EMISSION LINES IN  $\alpha$  AQUARI and  $\beta$  AQUARI

| A. $\alpha$ Aquarii |                |           |                   |         |                            | B. $\beta$ Aquarii |                |         |            |
|---------------------|----------------|-----------|-------------------|---------|----------------------------|--------------------|----------------|---------|------------|
| SWP 3587            |                | SWP 3610  |                   | $F_*^b$ | IDENT.                     | SWP 3646           |                |         |            |
| $\lambda$           | $f_{\oplus}^a$ | $\lambda$ | $f_{\oplus}^a$    |         |                            | $\lambda$          | $f_{\oplus}^a$ | $F_*^b$ | IDENT.     |
| 1237.2              | 2.3            | 1236.2    | 1.9               | 4.2+3   | N v $\lambda$ 1240         | 1231.2             | 1.6            | 3.7+3   | N v        |
| 1295.6b             | 5.3            | 1295.4    | 5.3               | 1.1+4   | Fe II+S I $\lambda$ 1296   | 1292.2             | 2.7            | 6.2+3   | Fe II, S I |
| 1304.0              | 30             | 1302.8    | 29                | 5.9+4   | O I $\lambda$ 1303         | 1300.4             | 15             | 3.4+4   | O I        |
| 1333.6              | 1.8            | 1334.8    | 1.7               | 3.5+3   | C II $\lambda$ 1335        | 1330.4             | 1.4            | 3.2+3   | C II       |
| 1335.0              | 2.6            | 1356.0    | 2.9               | 5.5+3   | O I $\lambda$ 1357         | 1351.4             | 2.0            | 4.6+3   | O I        |
| 1394.4              | 1.4            | 1394.2    | 1.5               | 2.9+3   | Si IV $\lambda$ 1394       | 1388.4             | 1.7            | 3.9+3   | Si IV      |
| 1402.6              | 1.3            | 1401.6    | 1.4               | 2.7+3   | Si IV $\lambda$ 1403       | 1401.6             | 0.9            | 2.1+3   | Si IV      |
| 1471.6              | 2.0            | 1473.8    | 2.5               | 4.5+3   | S I $\lambda$ 1475         | 1465.6             | 1.2            | 2.8+3   | S I?       |
| 1484.8              | 1.6            | 1487.0    | 2.0               | 3.6+3   | S I $\lambda$ 1488         | 1482.2             | 0.8            | 1.8+3   | S I        |
| 1527.6              | 1.9            | 1525b     | 1.6               | 3.5+3   | Si II $\lambda$ 1530       | 1495.2             | 0.6            | 1.4+3   | ....       |
| 1549.0              | 3.0            | 1548.8    | 3.3               | 6.3+3   | C IV $\lambda$ 1550        | 1521.6             | 1.4            | 3.2+3   | Si II      |
| 1557.2b             | (0.9)          | ....      | ....              | (1.8+3) | C I $\lambda$ 1560?        | 1545.4             | 2.9            | 6.7+3   | C IV       |
| 1642.8b             | 2.4            | 1641.6    | 1.6               | 4.0+3   | He II $\lambda$ 1640+Fe II | 1636.8             | 1.1            | 2.5+3   | He II      |
| 1658.4              | 2.1            | 1658.2    | 3.0               | 5.1+3   | C I $\lambda$ 1657         | 1652.4             | 1.8            | 4.1+3   | C I        |
| 1808.2              | 2.5            | 1809.4    | 2.7               | 5.2+3   | Si II $\lambda$ 1808       | 1802.0             | 1.1            | 2.5+3   | Si II      |
| 1818.8              | 6.4            | 1818.0    | O.E. <sup>c</sup> | 1.3+4   | Si II $\lambda$ 1817       | 1812.8             | 6.6            | 1.5+4   | Si II      |
| 1893.6b             | 6.7            | ....      | ....              | 1.3+4   | Si III $\lambda$ 1892      | ....               | ....           | ....    | ....       |
| 1909.2              | <3.5           | ....      | ....              | <7+3    | C III $\lambda$ 1909?      | ....               | ....           | ....    | ....       |

<sup>a</sup> In units of  $10^{-13}$  ergs  $\text{cm}^{-2}$   $\text{s}^{-1}$ .

<sup>b</sup> Mean stellar surface flux in units of ergs  $\text{cm}^{-2}$   $\text{s}^{-1}$ , where  $a + \alpha$  implies  $a \times 10^\alpha$ .

<sup>c</sup> O.E. = overexposure.

TABLE 3

MAGNESIUM II FLUXES AND RELATIVE VELOCITIES (absorption components)

| Star                    | Line | $V_1^a$ (km s $^{-1}$ ) | $V_2$ (km s $^{-1}$ ) | $f_{\oplus}^b$ | $f_{\oplus}^c$ |
|-------------------------|------|-------------------------|-----------------------|----------------|----------------|
| $\lambda$ Vel . . . . . | $k$  | -18.2                   | ...                   | 3.31-11        | ...            |
|                         | $h$  | -21.4                   | ...                   | 3.37-11        | ...            |
| $\alpha$ Aqr . . . . .  | $k$  | -15.0                   | -126.6                | 2.27-11        | (1.77-11)      |
|                         | $h$  | -26.3                   | -126.8                | 2.73-11        | (2.20-11)      |
| $\beta$ Aqr . . . . .   | $k$  | -19.8                   | -81.0                 | 1.92-11        | (1.12-11)      |
|                         | $h$  | -19.8                   | -68.0                 | 1.68-11        | (1.00-11)      |

<sup>a</sup> Resolution  $\sim 30$  km s $^{-1}$ ; estimated probable error in relative velocities  $\sim 10$  km s $^{-1}$ .

<sup>b</sup> Flux at Earth in ergs cm $^{-2}$  s $^{-1}$ .

<sup>c</sup> Fluxes corrected for maximum possible photospheric contribution.

interpretable as the wind velocity, requiring instead a disentangling of the P Cygni profile if the line-forming region is extended (cf. Bernat 1977). However, this will not result in major changes in the listed velocities.

The circumstellar shell structures appear to be semi-permanent. Optical spectra of the Ca II lines in  $\alpha$  Aqr and  $\beta$  Aqr taken over a period of years show absorption components with essentially the same velocity shifts.

The Mg II line fluxes listed have been calculated in two ways for the G supergiants. The first numbers listed are the total fluxes between the minimum flux points ( $k_1$  and  $h_1$ ). Linsky and Ayres (1978) consider that some photospheric emission also contributes to the flux in this wavelength range, which they estimate from model atmospheres. In the absence of supergiant models, we simply define a "continuum" by connecting the minimum points. The numbers in parentheses give the flux above the "continuum" line. The correct flux is clearly between the two values. For  $\lambda$  Vel the continuum correction is negligible.

### III. DISCUSSION

The presence of high-velocity Ca II and Mg II circumstellar shells in these G supergiants may be viewed as part of the overall trend noted by Reimers (1977) for wind terminal velocities to increase with increasing gravity. The presence of high-temperature ions in the short-wavelength spectra suggests that the presence of some hot gas in the wind is responsible for producing intermediate terminal velocities, lower than the solar wind, but substantially higher than those typical of cool supergiants. One possibility is that thermal expansion increases terminal velocities. An isothermal corona around  $\alpha$  Aqr with  $T \sim 5 \times 10^5$  K would have a sonic point near the stellar surface (using  $\log g \sim 1.1$  from Parsons and Bouw 1971, and  $R \sim 100 R_{\odot}$ ). From the observations of N v we know that the gas temperature rises to at least  $\sim 2 \times 10^5$  K, which suggests that thermal pressure is important.

However, it is unlikely that the hot gas directly responsible for the N v emission has a sufficient emission measure to influence greatly the terminal velocities. We adopt an order-of-magnitude estimate of the mass-loss rate  $\dot{M} \sim 2 \times 10^{-8} M_{\odot} \text{ yr}^{-1}$  from Sanner's (1976) scaling law. In order to get a mass-loss rate from our

observations, we would require an analysis of circumstellar lines in other wavelength regions to determine the ionization balance. From the terminal-velocity observations, the velocity of the hot gas must be  $v \lesssim 100$  km s $^{-1}$ . Assuming that the hot gas is in the vicinity of the stellar surface, the electron density is  $\gtrsim 10^8$  cm $^{-3}$ . To obtain the N v emission observed,  $n_e^2 h \sim 10^{25}$  cm $^{-5}$ , so  $h \lesssim 10^9$  cm  $\sim 10^{-4} R_{\star}$ . This suggests that the N v emission region is very narrow unless the mass-loss rate has been overestimated by two orders of magnitude, so this hot gas is very unlikely to contribute substantially to the expansion of the wind.

Gas at a much higher temperature,  $\gtrsim 10^6$  K, could have sufficient emission measure to influence the wind terminal velocity. We may make an estimate of coronal emission from observations of the  $\lambda 1640$  blend. Photons with  $55 \text{ eV} < h\nu < 100 \text{ eV}$  can ionize He $^+$ , and He II  $\lambda 1640$  is produced by ensuing recombination. From the treatment of Raymond, Noyes, and Stopa (1979) and the thermal emission spectrum of Raymond and Smith (1977), the assumption that the entire  $\lambda 1640$  flux is He II recombination radiation yields conservative upper limits to the X-ray flux of  $3 \times 10^5$  ergs cm $^{-2}$  s $^{-1}$  for coronal temperatures  $10^{5.8} < T < 10^{6.2}$  K, and  $1.5 \times 10^6$  ergs cm $^{-2}$  s $^{-1}$  for  $10^{5.5} < T < 10^{6.5}$  K (for  $\alpha$  Aqr). These fluxes imply  $n_e^2 h \lesssim 10^{28}$ . The emission measure result indicates an upper limit to coronal radiative losses of  $\sim 6$  times the kinetic energy losses in the wind, demonstrating that wind losses may significantly affect the thermal structure. The 0.25 keV X-ray flux at the Earth is predicted to be  $< 7 \times 10^{-12}$  ergs cm $^{-2}$  s $^{-1}$  (cf. Hartmann *et al.* 1979). Taking into account the probable contribution of Fe II to the  $\lambda 1640$  blend and absorption by the cool wind exterior to the corona may reduce this predicted upper limit substantially. X-ray observations can test these calculations and indicate the possible importance of thermal expansion on wind structure.

An alternative possibility is that the hot gas and mass loss arise from completely different regions on the stellar surface, and are not physically connected. High-dispersion UV spectra can in principle resolve this difficulty through velocity measurements, but will require very long exposures.

The surface fluxes in Mg II are 0.71 and 0.46 times the quiet-Sun value for  $\alpha$  Aqr and  $\beta$  Aqr, respectively.

However, the Mg II surface flux for  $\lambda$  Vel is only  $\sim 5.5 \times 10^{-2}$  times the quiet Sun. The surface fluxes in the lines at  $\lambda\lambda 1475, 1488$  are also down by a factor of 3 in  $\lambda$  Vel from the G supergiants, and the Si II and S I features  $\sim \lambda 1810$  are down by almost an order of magnitude. This suggests that the amount of mechanical heating present is critical to the development of transition regions, with larger mechanical energy fluxes leading to relative enhancements of high-temperature gas. Such an effect appears in dwarfs (Hartmann *et al.* 1979), where active stars have high-temperature emission lines enhanced more than lines from ions formed at relatively low temperatures. Since stars in the same position in the H-R diagram have varying levels of chromospheric activity, the position of the observed onset of transition

regions (Linsky and Haisch 1979) might be "smeared"; the observational evidence for this is growing (Dupree *et al.* 1979; Brown, Jordan, and Wilson 1979).

The existence of hybrid chromospheres and winds suggests a gradual transition from solar-type winds to supergiant winds, and indicates that theories incorporating solar-type behavior for stars of varying gravity may result in a more unified theory of mass loss in late-type stars.

We acknowledge useful conversations with R. Rosner. This work was supported in part by NASA grants NSG 7118 and NSG 7176 to the Harvard College Observatory.

## REFERENCES

- Abt, H. A., and Biggs, E. S. 1972, *Bibliography of Stellar Radial Velocities*, (Tucson: Kitt Peak National Observatory).  
 Barnes, T., and Evans, D. S. 1976, *M.N.R.A.S.*, **174**, 489.  
 Bernat, A. 1977, *Ap. J.*, **213**, 756.  
 Boggess, A., *et al.* 1978, *Nature*, **275**, 361.  
 Brown, A., Jordan, C., and Wilson, R. 1979, in *The First Year of IUE*, ed. A. J. Willis (London: University College London), p. 232.  
 Carpenter, K. G., and Wing, R. F. 1979, *Bull. AAS*, **11**, 419.  
 Deutsch, A. J. 1956, *Ap. J.*, **123**, 210.  
 ———. 1960, in *Stellar Atmospheres*, ed. J. G. Greenstein (Chicago: University of Chicago Press), p. 543.  
 Dupree, A. K., Black, J. H., Davis, R. J., Hartmann, L., and Raymond, J. C. 1979, in *The First Year of IUE*, ed. A. J. Willis (London: University College London), p. 217.  
 Hartmann, L., Davis, R., Dupree, A. K., Raymond, J., Schmidtke, P. C., and Wing, R. F. 1979, *Ap. J. (Letters)*, **233**, L69.  
 Holm, A. 1979, private communication.  
 Johnson, H. L., Mitchell, R. I., Iriarte, B., and Wisniewski, W. Z. 1966, *Comm. L.P.L.*, No. 63, p. 4.  
 Linsky, J. L., and Ayres, T. R. 1978, *Ap. J.*, **220**, 619.  
 Linsky, J. L., and Haisch, B. M. 1979, *Ap. J. (Letters)*, **229**, L27.  
 Mullan, D. J. 1978, *Ap. J.*, **226**, 151.  
 Parsons, S. B., and Bouw, G. 1971, *M.N.R.A.S.*, **152**, 133.  
 Raymond, J. C., Noyes, R. W., and Stopa, M. 1979, *Solar Phys.*, **61**, 271.  
 Raymond, J. C., and Smith, B. W. 1977, *Ap. J. Suppl.*, **35**, 419.  
 Reimers, D. 1977, *Astr. Ap.*, **57**, 395.  
 Sanner, F. 1976, *Ap. J. Suppl.*, **32**, 115.  
 Stencel, R. E. 1978, *Ap. J. (Letters)*, **223**, L37.  
 Weymann, R. 1962, *Ap. J.*, **136**, 844.  
 Wing, R. F. 1978, in *Proc. 4th Internat. Colloq. Ap.*, ed. M. Hack (Trieste), p. 683.

A. K. DUPREE, L. HARTMANN, and J. C. RAYMOND: Harvard-Smithsonian Center for Astrophysics, Cambridge MA 02138